Synthesis, microstructural characterization and transport properties of a new (Ti2Nb)AlC2 ternary nanolaminate carbide solid solution.

Mohammed Berrabah, T. Cabioc'H, Véronique Gauthier-Brunet, Patrick Chartier, Enrica Epifano, Sylvain Dubois

Journal of the European Ceramic Society 46 (2026) 117894

Contents lists available at ScienceDirect

Journal of the European Ceramic Society

journal homepage: www.elsevier.com/locate/jeurceramsoc

Synthesis, microstructural characterization and transport properties of a new $(Ti_2Nb)AlC_2$ ternary nanolaminate carbide solid solution.

M. Berrabah [a], T. Cabioc'h [a], V. Gauthier-Brunet [a], P. Chartier [a], E. Epifano [b], S. Dubois [a,*]

[a] PPRIME Institute, CNRS, Université de Poitiers, ENSMA, UPR 3346, SP2MI, TSA 41123, 86073 Poitiers cedex 9, France
[b] CIRIMAT, 4 allée Emile Monso, BP44362, Toulouse Cedex 4 31030, France

ARTICLE INFO

Keywords:
MAX phases
Solid Solution
Transport Properties
Hot Isostatic Pressing
Microstructure

ABSTRACT

A new $(Ti_2Nb)AlC_2$ MAX phase solid solution is synthesized by hot isostatic pressing a powder mixture of sub-stoichiometric titanium carbide, niobium and aluminum. It is demonstrated that the synthesis temperature and Al content are key parameters to obtain a large volume fraction of 312 MAX phase solid solution. Rietveld refinement allows determining the cell parameters which are shown to vary from one sample to another. Thus, $(Ti_2Nb)AlC_2$ is not a line compound but a disordered solid solution. The 312 MAX phase solid solution formation mechanism is discussed considering intermediate phases observed by scanning electron microscopy and analysed using energy dispersive X-ray spectroscopy. Finally, transport properties are characterized. It is demonstrated that electron-phonon coupling is more efficient than in Ti_3AlC_2 and Ti_3SiC_2.

1. Introduction

MAX phases are layered ternary carbides and nitrides with the general formula $M_{n+1}AX_n$ (where *M* is an early transition metal, *A* is an A-group element, and *X* is either carbon or nitrogen) [1–6]. These nanolaminated materials alternate layers of near-close-packed M_6X octahedra interleaved with layers of pure A-group element. In the M_4AX_3 or 413's (n = 3), three M_6X octahedra are interleaved between A layers [7,8]; in the M_3AX_2 or 312's (n = 2), two M_6X octahedra are interleaved between A layers [3]; and in the M_2AX or 211's phases (n = 1), one M_6X octahedra is interleaved between A layers [1–3]. This structural configuration endows MAX phases with an unusual combination of ceramic and metallic properties, including high thermal and electrical conductivity, excellent machinability, and good damage tolerance [6]. Among them, the Ti-based MAX phases have attracted significant interest due to their stability and mechanical performance at elevated temperatures [6].

In recent years, the development of MAX phase solid solutions has emerged as a strategic approach for tailoring physical properties through atomic-scale engineering. The synthesis of MAX phase solid solutions falls into three primary categories: (i) Molten salt processes [9,10], (ii) solid-state reactions [11,12] and (iii) physical vapor deposition (PVD) methods [13]. Although the synthesis of MAX phase solid solution is generally feasible, attaining high yields (>95 wt%), it presents challenges due to its synchronicity with other thermodynamically steady phases like carbides, nitrides, and intermetallic compounds. Challenges that commonly hinder preparation of homogeneous MAX phase solid solutions also include loss of volatile A-site elements (notably Al) at elevated temperatures. Solid solutions allow the partial substitution of elements on the *M*, *A*, or *X* sites, enabling the fine-tuning of characteristics such as hardness, thermal conductivity, oxidation resistance, and phase stability. As an example, Cabioc'h et al. [14] showed that when substituting 25 % of the Al atoms for Ge in Cr_2AlC, its thermal expansion becomes isotropic, presumably diminishing thermal stresses in the material. Studies on MAX phase solid solutions such as (TiNb)AlC have revealed that partial substitution of Ti with Nb leads to an increase in hardness and elastic modulus, suggesting a solid solution hardening effect [15]. An appreciable increase in fracture toughness is also observed in the $(Nb_{0.85}Zr_{0.15})_4AlC_3$ solid solution, from 6.6 ± 0.1 MPa/m$^{1/2}$ for pure Nb_4AlC_3 to 10.1 ± 0.3 MPa/m$^{1/2}$ for the solid solution [16]. It has also been demonstrated that doping with a low concentration of Zr can simultaneously improve the oxidation resistance and mechanical properties of Nb_4AlC_3 [17]. Substitution of Ti by Nb and Mo in Ti_3AlC_2 leads to an increase in electrical conductivity. Such an effect is attributed to an increase of the electronic density of states near the Fermi level, particularly significant when dopants are present at both the M and A sites [18].

Notably, when multiple principal elements are introduced,

* Corresponding author.
E-mail address: sylvain.dubois@univ-poitiers.fr (S. Dubois).

https://doi.org/10.1016/j.jeurceramsoc.2025.117894
Received 21 July 2025; Received in revised form 2 October 2025; Accepted 9 October 2025
Available online 11 October 2025

particularly on the *M* site, the resulting materials are referred to as high-entropy MAX phases. These high-entropy systems exhibit enhanced entropy-driven stabilization and often display improved mechanical and thermal properties compared to their single-element counterparts [19,20].

Another emerging direction in the study of MAX phases is their selective etching to produce two-dimensional (2D) materials known as MXenes. These are obtained by removing the *A* element - typically through chemical exfoliation - while retaining the layered $M_{n+1}X_n$ framework. MXenes derived from solid solution and high-entropy MAX phases open up vast compositional design spaces and tunable properties that can be exploited in energy storage, electromagnetic interference shielding, catalysis, and more [21,22]. Multiple transition metals in the *M* site can lead to MXenes with unique surface chemistries, higher configurational entropy and potentially enhanced multifunctional properties. Thus, the development of Ti_2NbAlC_2 and similar solid solutions is not only valuable for their bulk properties, but also for their promise as precursors for novel, multifunctional MXenes.

This work focuses on the powder metallurgy synthesis and transport properties characterization of a new $(Ti_2Nb)AlC_2$ solid solution. The study involves a detailed investigation of the phase formation, microstructural features, and key transport properties of this MAX phase solid solution, thereby contributing to the broader understanding of compositional engineering in MAX phases and their potential in advanced structural applications.

2. Experimental details

This work was performed using powder mixtures of sub-stoichiometric titanium carbide ($TiC_{0.91}$, Good Fellow, 50–150 μm, 99.8 %), niobium (Alfa Aesar, <44 μm, 99.8 %) and aluminum (Alfa Aesar, <44 μm, 99.5 %) to yield a final composition with the appropriate stoichiometry 2:1:1.10–1.20 ($2TiC_{0.91}$:Nb:Al). Al excess was used to compensate Al vaporization during synthesis. The powders were thoroughly ball-mixed under dry air in a tridimensional Turbula® mixer for 20 min in order to ensure good mixing and to break up agglomerates. The powder mixture was then uniaxially cold-pressed (35 MPa) into a cylindrical green pellet (20 mm in diameter). The pellet was encapsulated into a glass container under primary vacuum to prevent oxidation during the subsequent heat treatment. An isostatic Ar pressure of 120 MPa was thus applied at temperature in the range 1450–1610°C during 4 h using a Hot Isostatic Press (ACB-HIP6).

After HIPing, the sample was machined to remove the encapsulating glass container, sliced using a diamond wheel, and roughly polished using SiC paper for microscopic observations. The latter were performed using a scanning electron microscope (SEM, JEOL 7001F-TTLS) equipped with an Energy Dispersive X-ray Spectrometer (EDXS, Oxford Isis 300) for chemical analysis. X-ray Diffraction (XRD) experiments were carried out on a Bruker D8 Advance diffractometer using the Cu K_α radiation (Bragg-Brentano geometry) for phase identification. Rietveld refinement was systematically performed on the samples synthesized at different temperatures to get the weight fraction of the present phases and the cell parameters of the Ti_2NbAlC_2 MAX phase.

The samples were cut into parallelepipeds with a section of approximately 2 mm^2 and a 8 mm length. Resistivity measurements were performed with a four-probe technique using the resistivity option of the Physical Property Measurement System (PPMS) by Quantum Design. A current of 8 mA was applied in order to reach a resistance of a few mΩ at Room Temperature (RT). Temperature was decreased slowly from RT to 5 K and resistance was measured continuously. Magnetoresistance was measured at 2, 100, 200, and 300 K for magnetic field varying in the range [0−9] T. Thermal conductivity was measured using the Thermal Transport Option (TTO) of the PPMS. The TTO system measures thermal conductivity by applying heat from the heater shoe in order to create a user-specified temperature differential between the two thermometer shoes. The TTO system dynamically models the thermal response of the sample to the low-frequency, square-wave heat pulse, thus expediting data acquisition. TTO can then calculate thermal conductivity directly from the applied heater power (about 50 mW at RT), resulting ΔT, and sample geometry.

Thermodynamic calculations were performed using the Thermo-Calc software and the TCHEA8 database from Thermo-Calc. The pressure was fixed at 10^5 bar. The nominal composition of the MAX phase was entered and calculations were performed as a function of the temperature.

3. Results and discussion

XRD patterns recorded on samples synthesized using HIPing technique at 1450, 1550, 1580 and 1610°C from a powder reactant mixture whose composition is $2TiC_{0.91}$:Nb:1.1Al are plotted in Fig. 1. The proportion of the different phases, determined using Rietveld refinement, is reported in Table 1. Note that the composition of the different phases identified by XRD was measured using EDXS analyses. One can observe in Table 1 that alumina is only detected at the lowest temperatures (1450 and 1485°C) and at 1595°C. Alumina is nevertheless observed by SEM for all temperatures (see below). The reason is unclear. It may result from an insufficient alumina content to be detected by X-Rays and/or from the presence of some amorphous alumina.

At 1450°C, $(Ti_{1.2}Nb_{0.8})Al_{0.9}C_{1.0}$ (further called 211 MAX phase), $Ti_{0.6}C_{0.4}$, $(Ti_{0.4}Nb_{0.1})C_{0.5}$ and $(Ti_{0.2}Nb_{0.9})Al_3$ are the main phases detected. When the synthesis temperature increases from 1450°C to 1580°C, the fraction of these different phases decreases whereas the fraction of the $(Ti_{1.9–2.1}Nb_{1.0–1.2})Al_{0.9}C_{1.8–2.0}$ phase (further called 312 MAX phase) increases. The 312 MAX phase is the main phase present (97.6 wt%) at 1580°C. When the synthesis temperature increases from 1580°C to 1610°C, the fraction of the 312 phase decreases whereas the fraction of 211 MAX phase, $Ti_{0.6}C_{0.4}$ and $(Ti_{0.4}Nb_{0.1})C_{0.5}$ increases.

Fig. 2 shows the variation of the 312 phase content as a function of the HIP synthesis temperature; the aluminum excess is 10 at%. XRD results suggest that the $(Ti_{1.9–2.1}Nb_{1.0–1.2})Al_{0.9}C_{1.8–2.0}$ phase is formed in the 1450–1580°C temperature range whereas it decomposes at higher temperature.

X-ray diffractogram recorded on the samples synthesized at 1580°C for an Al excess of 10 at% and corresponding Rietveld refinement are reported in Fig. 3. In the Wycoff notations, it exists four inequivalent sites in the hexagonal $P6_3/mmc$ space group for 312 MAX phases: M_I in 2a, M_{II} in 4 f, A in 2b and X in 4 f. For the atoms in 4 f positions, the ideal values of the two internal dimensionless parameters z/c are 1/8 = 0.125 and 1/16 = 0.0625 for M_{II} and X respectively. From our analysis, $(Ti_{1.9–2.1}Nb_{1.0–1.2})Al_{0.9}C_{1.8–2.0}$ departs from the ideal stacking because we obtain z/c = 0.13 for M_{II} and z/c = 0.072 for C atoms, a behavior already observed in MAX phases [23–25]. The mean value of the cell parameters that we get from Rietveld refinement performed on all synthesized samples are a = 0.310087(6) nm and c = 1.86139(6) nm whereas corresponding standard deviations are 0.0001 nm and 0.0006 nm. The large difference between the standard deviation and the cell parameters uncertainty allows affirming that $(Ti_{1.9–2.1}Nb_{1.0–1.2})Al_{0.9}C_{1.8–2.0}$ is a disordered solid solution and not a line compound. It is also interesting to note that Rietveld refinement of XRD data is a powerful tool to determine a preferential position of the Nb atoms on the M_I or M_{II} sites thank to quite large difference of atomic number of Ti and Nb. In the present case, the refinement of the occupation for these two sites always leads to 1/3 of Nb and 2/3 of Ti confirming thus the formation of a disordered solid solution. Sample density measurement, performed via apparent volume and weight measurements, leads to a (98.1 ± 0.2) % relative density for the sample synthesized at 1580°C.

Table 2 reports the content (in weight %) of the different phases present as a function of the aluminum content in the initial reactant mixture ($2TiC_{0.91}$:Nb:1.10–1.20Al) for HIPing treatment performed at 1580°C. It is shown, from Rietveld refinement, that the alumina content is minimum and the 312 MAX phase content is maximum for an aluminum excess of 10 at%. For aluminum excess of 15 or 20 at%, the

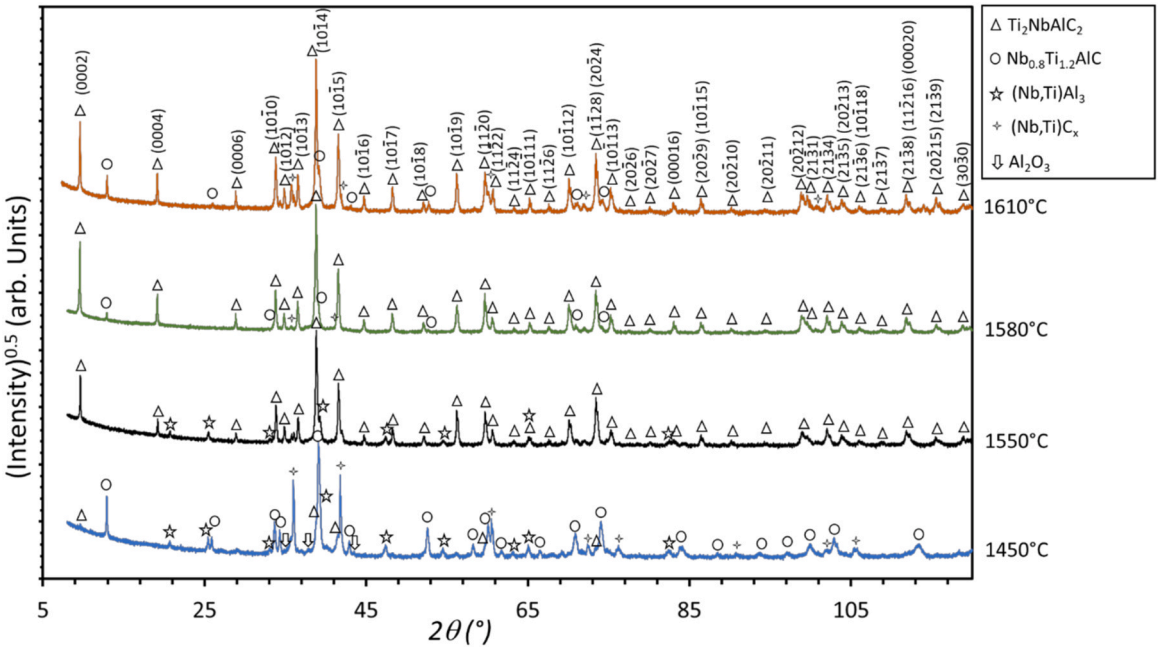

Fig. 1. XRD patterns recorded on HIPed-samples synthesized at 1450, 1550, 1580 and 1610°C with an aluminum excess of 10 at%.

Table 1
Weight % of the different phases present in the HIPed samples synthesized in the temperature range 1450–1610°C with a reactant mixture of $2TiC_{0.91}$:Nb:1.1Al.

T (°C)	312 MAX phase solid solution $(Ti_{1.9-2.1}Nb_{1.0-1.2})Al_{0.9}C_{1.8-2.0}$	211 MAX phase solid solution $(Ti_{1.2}Nb_{0.8})Al_{0.9}C_{1.0}$	$Ti_{0.6}C_{0.4}$ and $(Ti_{0.4}Nb_{0.1})C_{0.5}$ carbides	$(Ti_{0.2}Nb_{0.9})Al_3$ intermetallic	Al_2O_3
1450	8.0	32.8	34.9	21.2	3.1
1485	43.3	13.0	13.0	28.0	2.7
1550	86.0	0.0	3.0	11.0	0.0
1580	97,6	1.2	1.2	0.0	0.0
1595	82.4	8.9	4.1	3.6	1.0
1610	80.8	9.2	10.0	0.0	0.0

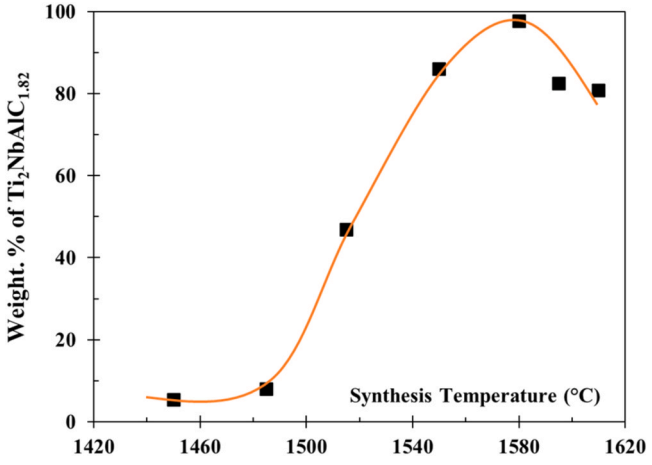

Fig. 2. 312 phase-weight content, determined from Rietveld refinement, as a function of the HIP synthesis temperature. Aluminum excess is10 at%.

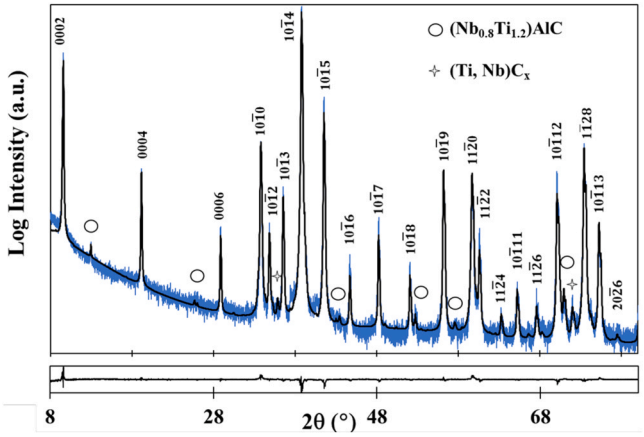

Fig. 3. XRD diagram recorded on the sample synthesized at 1580°C with an aluminum excess of 10 at%. (blue line) and corresponding Rietveld refinement (black line). Beneath, the difference between refined and experimental diffractograms. Miller indices are given for the 312 MAX phase.

312 MAX phase content decreases whereas the alumina content increases.

SEM micrographs of the samples HIPed at 1550, 1580 and 1610°C with an excess of aluminum of 10 at% are shown respectively in Fig. 4a, b, c and d. EDXS performed at low acceleration voltage (5–10 KeV) allows determining the chemical composition of the different contrasted areas. After HIPing at 1550°C (Fig. 4a), the large black regions corresponding to $Ti_{0.6}C_{0.4}$ are surrounded by a mixed $(Ti_{0.4}Nb_{0.1})C_{0.5}$ carbide (dark grey contrast). The main areas with the lighter contrast correspond to $(Ti_{1.9-2.1}Nb_{1.0-1.2})Al_{0.9}C_{1.8-2.0}$ MAX phase grains. The dark grey region, located at the 312 MAX phase grain boundaries, consists in $(Ti_{0.2}Nb_{0.9})Al_3$ intermetallic whereas the small black areas are Al_2O_3. After HIPing at 1580°C, the main grey contrasted areas in

Table 2
Content (in weight %) of the phases present as a function of the aluminum content in the initial $2TiC_{0.91}$:1 Nb:1.10–1.20Al reactant mixture after HIPing treatment at 1580°C.

Al content in the reactant mixture	$(Ti_{1.9-2.1}Nb_{1.0-1.2})Al_{0.9}C_{1.8-2.0}$	$Ti_{0.6}C_{0.4}$ and $(Ti_{0.4}Nb_{0.1})C_{0.5}$	$(Ti_{1.2}Nb_{0.8})Al_{0.9}C_{1.0}$	Al_2O_3
1.10	97.6	1.2	1.2	0
1.15	96.6	0.7	1.2	1.5
1.20	96.0	0.6	1.4	2.0

Figs. 4b and 4c correspond to $(Ti_{2.0}Nb_{1.0})Al_{0.9}C_{2.0}$ MAX phase. Fig. 4c shows that Al_2O_3 (black contrast) and $(Ti_{1.9}Nb_{1.1})Al_{1.3}C_{1.7}$ containing Si (white contrast) are present at the grain boundaries of the 312 MAX phase whereas some unreacted $Ti_{0.6}C_{0.4}$ (darker grey contrast) is still present. After HIPing at 1610°C, the lighter grey contrast of Fig. 4d corresponds to $(Ti_{2.1}Nb_{1.1})Al_{0.9}C_{1.9}$ MAX phase. Black regions, dark grey and white contrasted areas are respectively Al_2O_3, $(Ti_{0.4}Nb_{0.1})C_{0.4}$ and/or $Ti_{0.6}C_{0.4}$ carbides and $(Ti_{1.2}Nb_{0.8})Al_{0.9}C_{1.0}$ MAX phase.

Finally, from EDXS measurements, it is demonstrated that $(Ti_{1.9-2.1}Nb_{1.0-1.2})Al_{0.9}C_{1.8-2.0}$ MAX phase solid solution is formed in the 1450–1580°C temperature range. From XRD and EDXS analyses, it has been shown that intermediate phases consist in $Ti_{0.6}C_{0.4}$ and $(Ti_{0.4}Nb_{0.1})C_{0.5}$ carbides, as well as $(Ti_{0.2}Nb_{0.9})Al_3$ intermetallic and $(Ti_{1.2}Nb_{0.8})Al_{0.9}C_{1.0}$ 211 MAX phase. For temperatures in the range [1450–1550°C], the $(Ti_{1.2}Nb_{0.8})Al_{0.9}C_{1.0}$ content decreases up to 0 wt% at 1550°C (see Table 1). The carbides and $(Ti_{0.2}Nb_{0.9})Al_3$ intermetallic contents decrease up to 1580°C. At this temperature, there is no more aluminides whereas the carbides content reaches a few percent. Thus, one can conclude that the formation of the $(Ti_{2.1}Nb_{1.1})Al_{0.9}C_{1.9}$ solid solution mainly results from the reaction between the $(Ti_{1.2}Nb_{0.8})Al_{0.9}C_{1.0}$ solid solution and the carbides for temperatures in the range [1450–1550°C]. At higher temperature [1550–1580°C], the formation of the $(Ti_{2.1}Nb_{1.1})Al_{0.9}C_{1.9}$ solid solution mainly results from the reaction between the $(Ti_{0.2}Nb_{0.9})Al_3$ intermetallic and the carbides. Nevertheless, thermodynamic calculation of the phase fraction as a function of the temperature would be necessary to confirm such an hypothesis. Above 1580°C, the results demonstrate that the 312 MAX phase solid solution starts to decompose since $(Ti_{0.4}Nb_{0.1})C_{0.4}$, $Ti_{0.6}C_{0.4}$ carbides and $(Ti_{1.2}Nb_{0.8})Al_{0.9}C_{1.0}$ 211 MAX phase are formed. This result can be qualitatively compared with the thermodynamic calculations of Fig. 5, showing the variation of the molar phase fractions as a function of the temperature, for a composition of 3Ti-1Al-2C. Niobium was not included in the calculation because the database does not describe any MAX phase in the Nb-Al-C system, nor does any other commercially available database. Fig. 5 shows that Ti_3AlC_2 starts to decompose above 1646°C, leading to the formation of Ti_2AlC, TiC and a liquid phase. Such a calculation is in compatible agreement with experimentally observed decomposition of Ti_3AlC_2 in Ti_2AlC and TiC [26]. The differences between the experimental evidences and the calculation- i.e. the sligh difference in the decomposition temperature and the absence of a liquid phase- are not surprising considering that Nb is not included in the calculation. The MAX phases are moreover known to undergo decomposition into their respective binary MX phases by dissociating the A element at compound-specific temperatures and in various atmospheres [26–29]. The major driving force leading to such a thermal decomposition is the high vapour pressure of the A element, which diffuses out of the MAX phase grains, evaporating above a certain threshold temperature [30]. Thus, it is not surprising that, at high temperature, the 312 $(Ti_{2.1}Nb_{1.1})Al_{0.9}C_{1.9}$ solid solution is less stable than the 211 $(Ti_{1.2}Nb_{0.8})$

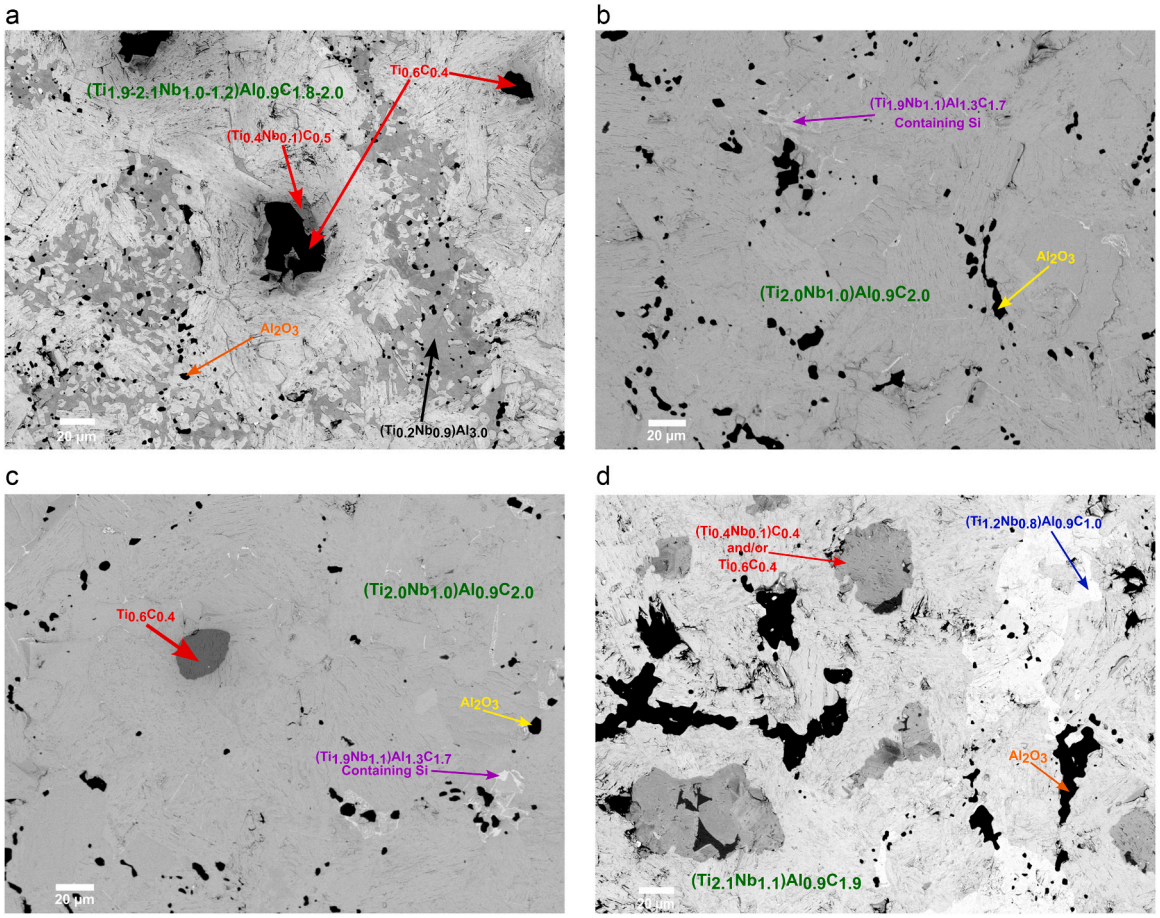

Fig. 4. SEM micrographs, in back-scattered mode, of the samples HIPed at 1550°C (a), 1580°C (b, c) and 1610°C (d). Al content is 1.1.

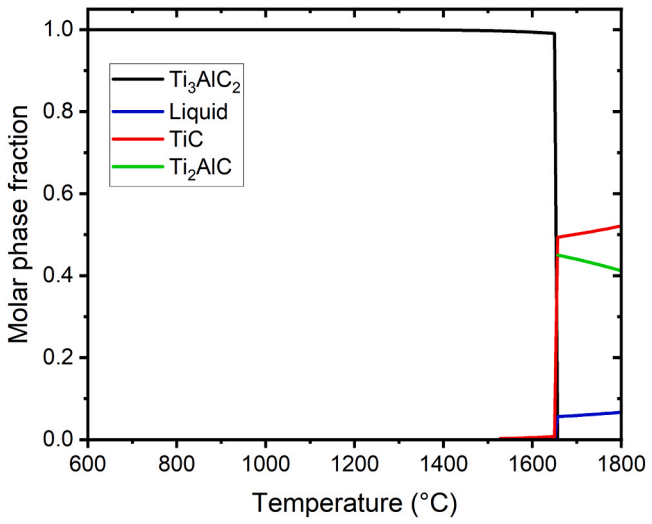

Fig. 5. Calculated variation of the molar phase fractions as a function of the temperature, for a composition of 3Ti-1Al-2C.

$Al_{0.9}C_{1.0}$ solid solution in equilibrium with corresponding carbides.

Fig. 6a shows the variation of the Ti_2NbAlC_2 resistivity as a function of temperature. The residual resistivity due to the electron-impurity and electron-defect scattering is quite large (about 77 μΩ.cm) whereas the slope of the linear variation (0.09 μΩ.cm.K^{-1}) which is related to the electron-phonon interaction is in the same range as the ones determined on other MAX phases (0.07–0.1 μΩ.cm.K^{-1}) [31–33]. In order to get a

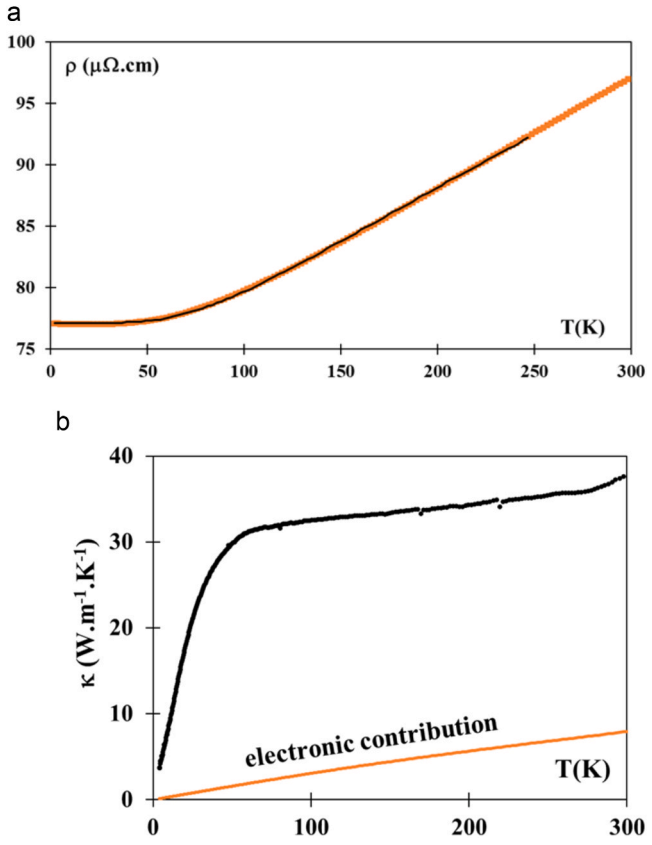

Fig. 6. (a) $(Ti_{1.9-2.1}Nb_{1.0-1.2})Al_{0.9}C_{1.8-2.0}$ resistivity variation with temperature and corresponding modelisation using the Bloch-Grüneisen model (see text), (b) variation, with temperature, of the $(Ti_{1.9-2.1}Nb_{1.0-1.2})Al_{0.9}C_{1.8-2.0}$ thermal conductivity (black line) and of the electronic contribution to the thermal conductivity (orange line, see text).

quantitative understanding of these scattering processes, the temperature dependent electrical resistivity of the sample is analyzed in terms of the Boltzmann transport theory using the Bloch-Grüneisen (BG) model [34,35]:

$$\rho_{B-G-M} = \rho_{residual} + \rho(\theta_{BG}).\frac{T^5}{{\theta_{BG}}^5}\int_0^{\theta_{BG}/T}\frac{x^5.dx}{(e^x-1)(1-e^{-x})}$$

where $\rho_{residual}$ is the residual resistivity due to the electron-impurity and electron-defect scattering and the second term is the temperature-dependent intrinsic resistivity. θ_{BG} is the effective Debye temperature determined from experimental resistivity data by the BG formula. $\rho(\theta_{BG}) = \frac{4\pi\lambda_{trace}\omega_D}{\varepsilon_0{\omega_p}^2}$ is the resistivity at the effective Debye temperature, λ_{trace} is the electron-phonon coupling constant, $\omega_D = \theta_{BG}.k_B/\hbar$ is the Debye frequency and ω_p is the Drude plasma frequency. The Drude plasma frequencies corresponding to the two components of the Ti_3SiC_2 dielectric tensor (i.e. ω_p^{xx} and ω_p^{zz}) have been obtained from linearized augmented plane wave (LAPW) electronic band structure calculations [36]. It is worth noticing that the value deduced from the trace of the dielectric tensor, $\hbar\omega_p = 4.0$ eV for Ti_3SiC_2, was in very good agreement with that obtained from monochromated EELS experiments performed on polycrystalline Ti_3SiC_2 ($\hbar\omega_p = 4.12$ eV) [37]. Monochromated EELS experiments performed on polycrystalline Ti_3AlC_2 gives $\hbar\omega_p = 5.1$ eV [37].

The only two free-parameters $(\rho(\theta_{BG}) \text{and} \theta_{BG})$ involved in the BG model were then adjusted to minimize the relative error defined as $(\rho^{EXP} - \rho^{FIT})/\rho^{EXP}$. Fig. 5a shows the experimental and calculated electrical resistivity variations as a function of temperature for the Ti_2NbAlC_2 sample. The value of θ_{BG} determined from the fit is 500 K which is in compatible agreement with Debye temperature in the range [420–800 K] found in reference [38]. Such a value of the Debye temperature associated to a plasma frequency of $\hbar\omega_p = 4.5$ eV (an average value of the one determined on Ti_3SiC_2 and Ti_3AlC_2 [27]) allows determining an electron-phonon coupling constant of 0.78. Such a value is higher than the one determined on Ti_3SiC_2 (0.46) [36] which is in compatible agreement with the slopes dρ/dT that is larger for Ti_2NbAlC_2 (0.09 μΩ.cm.K^{-1}) than for Ti_3SiC_2 (0.07 μΩ.cm.K^{-1}) [31].

Fig. 6b shows the variation, with temperature, of the Ti_2NbAlC_2 thermal conductivity and of the electronic contribution to the thermal conductivity. The electronic contribution to the thermal conductivity has been calculated using the Wiedemann-Franz law. The Wiedemann-Franz law states that the ratio of the electronic contribution of the thermal conductivity to the electrical conductivity is proportional to the temperature and to the Lorentz number. The thermal conductivity at RT is as low as 40 W.$m^{-1}K^{-1}$ which is comparable to the ones that can be measured on other MAX phases [39–42]. At RT, the electronic contribution to the thermal conductivity is about 21 % which implies that the main contribution to the thermal conductivity is due to phonons. Such a large contribution of phonons largely depends on the MAX phases [39–42].

Fig. 7 shows the magnetoresistance (MR) as a function of the square of the ratio between the magnetic field and the zero-field resistivity. First of all, one can notice that the magnetoresistance is very small (about 0.04 % at 2 K and 9 T). Moreover, a single curve is observed in Fig. 6 which implies that the Kohler's rule is obeyed [43,44]. From the Kohler's rule, one can deduce that $MR \sim B^2 . (n.e.\mu(T, H = 0))^2$ where n, e and μ are respectively the charge carrier density, the electron charge and the charge carrier mobility at zero field and at the temperature T. Thus, it demonstrates that the MR is proportional to the square of the charge carrier mobility.

4. Summary and conclusion

A powder mixture of sub-stoichiometric titanium carbide, niobium and aluminum is hot isostatically pressed at 1450–1660°C/120 MPa/

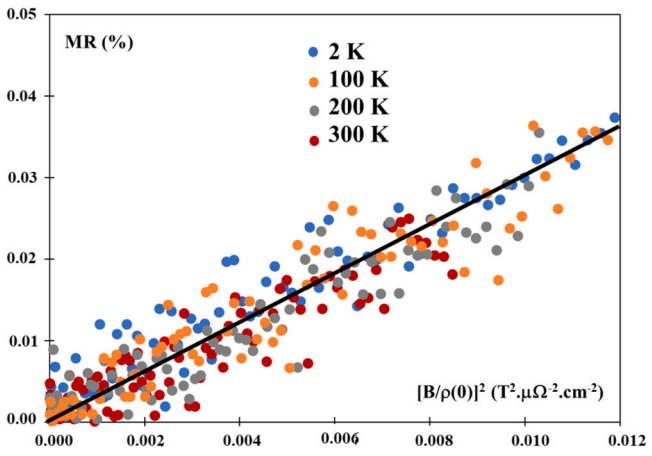

Fig. 7. Magnetoresistance (MR) variation versus $[B/\rho(0)]^2$.

4 h. It is demonstrated that $(Ti_{1.9–2.1}Nb_{1.0–1.2})Al_{0.9}C_{1.8–2.0}$ is formed in the 1450–1580°C temperature range, from intermediate phases such as carbides, intermetallic and the 211 MAX phase solid solution. The synthesis temperature and Al content are key parameters to obtain a large volume fraction of $(Ti_{1.9–2.1}Nb_{1.0–1.2})Al_{0.9}C_{1.8–2.0}$. Using 10 at% excess of aluminum at 1580°C allow optimizing the 312 MAX phase solid solution content (97.6 wt%). Above 1580°C, it seems that $(Ti_{1.9–2.1}Nb_{1.0–1.2})Al_{0.9}C_{1.8–2.0}$ starts to decompose.

Transport property measurements show that electrical resistivity is quite high compared to the ones obtained on other MAX phases. Such a result is due to the large residual resistivity and to the electron-phonon coupling constant which is higher than the ones determined in other MAX phases. It is also demonstrated that the MR follows the Kohler's rule which implies that the MR is proportional to the square of the charge carrier mobility. Finally, the main contribution to the thermal conductivity is shown to be due to phonons.

CRediT authorship contribution statement

Mohammed Berrabah: Writing – original draft, Visualization, Investigation, Formal analysis, Conceptualization.**Thierry Cabioc'h:** Writing – review & editing, Supervision, Formal analysis. **Véronique Gauthier-Brunet:** Writing – review & editing, Supervision, Formal analysis. **Patrick Chartier:** Writing – review & editing, Supervision, Formal analysis. **Enrica Epifano:** Formal analysis, Investigation, Writing – review & editing. **Sylvain Dubois:** Writing – review & editing, Supervision, Project administration, Funding acquisition, Conceptualization.

Declaration of Competing Interest

The authors declare that they have no known competing financial interests or personal relationships that could have appeared to influence the work reported in this paper.

Acknowledgments

This work was supported by the French Gouvernement program "Investissements d'Avenir" EUR INTREE, reference ANR-18-EURE-0010. This work was supported by the ANR HEIRMAX, ANR-23-CE08–0005–04.

References

[1] W. Jeitschko, H. Nowotny, F. Benesovsky, Kohlenstoffhaltige ternäre verbindungen (H-Phase), Mon. Chem. 94 (1963) 672, https://doi.org/10.1007/BF00913068.

[2] W. Jeitschko, H. Nowotny, F. Benesovsky, *Die h-phasen ti$_2$*TlC, Ti$_2$PbC, Nb$_2$InC, Nb$_2$*snc und ta$_2$*GaC, Mon. Chem. 95 (1964) 431, https://doi.org/10.1007/BF00901306.

[3] W. Jeitschko, H. Nowotny, *Die kristallstruktur von ti$_3$sic$_2$* - ein neuer Komplexcarbid-Typ, Mon. Chem. 98 (1967) 329, https://doi.org/10.1007/BF00899949.

[4] H. Haschke, H. Nowotny, F. Benesovsky, Neodym-Perowskitcarbide und -nitride, Mon. Chem. 98 (1967) 2157–2163, https://doi.org/10.1007/BF00902410.

[5] V.H. Nowotny, Strukturchemie einiger verbindungen der Übergangsmetalle mit den elementen C, si, ge, sn, Prog. Solid State Chem. 5 (1971) 27–70, https://doi.org/10.1016/0079-6786(71)90016-1.

[6] M.W. Barsoum, The $M_{n+1}AX_n$ phases: a new class of solids; thermodynamically stable nanolaminates, Prog. Solid State Chem. 28 (2000) 201–281, https://doi.org/10.1016/S0079-6786(00)00006-6.

[7] M.W. Barsoum, L. Farber, I. Levin, A. Procopio, T. El-Raghy, A. Berner, High-resolution transmission electron microscopy of ti$_4$a lN $_3$, or Ti$_3$al$_2$n$_2$ revisited, J. Am. Ceram. Soc. 82 (1999) 2545–2547, https://doi.org/10.1111/j.1151-2916.1999.tb02117.x.

[8] C.J. Rawn, M.W. Barsoum, T. El-Raghy, A. Procopio, C.M. Hoffmann, C. Hubbard, Structure of ti$_4$a lN $_3$ - a layered $M_{n+1}alx_n$ nitride, Mater. Res. Bull. 35 (2000) 1785, https://doi.org/10.1016/S0025-5408(00)00383-4.

[9] Jesus Gonzalez-Julian, Processing of MAX phases: from synthesis to applications, J. Am. Cer. Soc. 104 (2) (2020), https://doi.org/10.1111/jace.17544.

[10] L. Hu, X. Luo, Q. Jin, K. Hu, Y. Song, Molten salt electrolysis synthesis of high-purity nanostructured $(v_xcr_{1-x})_2$AlC solid solutions with tunable cr/V ratios, J. All. Com. 1037 (2025) 182257, https://doi.org/10.1016/j.jallcom.2025.182257.

[11] W. Yu, V. Mauchamp, T. Cabioc'h, D. Magne, L. Gence, L. Piraux, V. Gauthier-Brunet, S. Dubois, Solid solution effects in ti$_2$al(c$_x$n$_y$) MAX phases: synthesis, microstructure, electronic structure and transport properties, Acta Mater. 80 (2014) 421–434, https://doi.org/10.1016/j.actamat.2014.07.064.

[12] L. Aouchiche, D. Eyidi, V. Brunet, M. Nechiche, S. Dubois, Synthesis and characterization of a new $(ti_{1-y}cu_y)_2(Al_{1-x}cu_x)$C MAX phase solid solution, Open Ceram. 17 (2024) 100530, https://doi.org/10.1016/j.oceram.2023.100530.

[13] C. Azina, B. Tunca, A. Petruhins, B. Xin, M. Yildizhan, P.O.Å. Persson, J. Vleugels, K. Lambrinou, J. Rosén, P. Eklund, Deposition of max phase containing thin films from a (ti,zr)2alc compound target, Appl. Surf. Sci. 551 (2021) 149370, https://doi.org/10.1016/j.apsusc.2021.149370.

[14] T. Cabioc'h, P. Eklund, V. Mauchamp, M. Jaouen, M.W. Barsoum, Tailoring of the thermal expansions of the max phases in the $cr_2(Al_{1-x},Ge_x)$C system, J. Eur. Ceram. Soc. 33 (2013) 897–904, https://doi.org/10.1016/j.jeurceramsoc.2012.10.008.

[15] G. Kubicki, J. Wiśniewski, S.A. Tsipas, A. Kania, A. Patalas, J. Jakubowicz, D. Garbiec, Synthesis of ternary and quaternary MAX phases in Ti/Cr/Nb/V-Al-C system by high energy ball milling and pressureless spark plasma sintering, J. Alloy. Compd. 1024 (2025) 180272, https://doi.org/10.1016/j.jallcom.2025.180272.

[16] T. Lapauw, D. Tytko, K. Vanmeensel, S. Huang, P.P. Choi, D. Raabe, E.N. Caspi, O. Ozeri, M. to Baben, J.M. Schneider, K. Lambrinou, J. Vleugels, $(Nb_x, Zr_{1-x})_4alc_3$ max phase solid solutions: processing, mechanical properties, and density functional theory calculations, Inorg. Chem. 55 (2016) 5445–5452, https://doi.org/10.1021/acs.inorgchem.6b00484.

[17] G. Liu, Z. Li, W. Gao, D. Zhao, B. Sun, W. Su, M. Yan, Y.D. Fu Liu, Oxidation mechanism and mechanical properties of substitutional transition metal modified Nb_4AlC_3: a first-principles density functional theory study, Ceram. Int. 49 (2023) 29141–29154, https://doi.org/10.1016/j.ceramint.2023.06.194.

[18] F.M. Oliveira, N. Amousa, A. Subramani, J. Luxa, C. Senthil, Z. Sofer, J. Gonzalez-Julian, Maximizing potential applications of max phases: sustainable synthesis of multielement ti_3alc_2, Inorg. Chem. 63 (2024) 14851–14859, https://doi.org/10.1021/acs.inorgchem.4c00648.

[19] J.W. Yeh, S.K. Chen, S.J. Lin, J.Y. Gan, T.S. Chin, T.T. Shun, C.H. Tsau, S.Y. Chang, Nanostructured high-entropy alloys with multiple principal elements: novel alloy design concepts and outcomes, Adv. Eng. Mater. 6 (2004) 299–303, https://doi.org/10.1002/adem.200300567.

[20] J. Brechtl, C. Lee, P.K. Liaw, High-entropy materials: fundamentals and applications, J. Mater. Res. Technol. 23 (2023) 5967–5971, https://doi.org/10.1016/j.jmrt.2023.02.189.

[21] M. Naguib, M. Kurtoglu, V. Presser, J. Lu, J. Niu, M. Heon, L. Hultman, Y. Gogotsi, M.W. Barsoum, Two-Dimensional nanocrystals produced by exfoliation of Ti_3AlC_2, Adv. Mater. 23 (2011) 4248–4253, https://doi.org/10.1002/adma.201102306.

[22] J. Halim, S. Kota, M.R. Lukatskaya, M. Naguib, M.Q. Zhao, E.J. Moon, J. Pitock, J. Nanda, S.J. May, Y. Gogotsi, M.W. Barsoum, Synthesis and characterization of 2D molybdenum carbide (MXene), Adv. Funct. Mater. 26 (2016) 3118–3127, https://doi.org/10.1002/adfm.201505328.

[23] G. Hug, M. Jaouen, M.W. Barsoum, X-ray absorption spectroscopy, eels, and full-potential augmented plane wave study of the electronic structure of ti_2alc, ti_2AlN, nb_2alc, and $(ti_{0.5}nb_{0.5})_2alc$, Phys. Rev. B 71 (2005) 024105, https://doi.org/10.1103/PhysRevB.71.024105.

[24] G. Hug, Electronic structures and composition gaps among the ternary carbides ti_2mc, Phys. Rev. B 74 (2006) 184113, https://doi.org/10.1103/PhysRevB.74.184113.

[25] S. Dubois, T. Cabioc'h, P. Chartier, V. Gauthier, M. Jaouen, A new ternary nanolaminate carbide: ti_3snc_2, J. Am. Ceram. Soc. 90 (2007) 2642–2644, https://doi.org/10.1111/j.1551-2916.2007.01766.x.

[26] W.K. Pang, I.M. Low, B.H. O'Connor, A.J. Studer, V.K. Peterson, Z.M. Sun, J. P. Palmquist, Comparison of thermal stability in MAX 211 and 312 phases, J. Phys. Conf. Ser. 251 (2010) 012025, https://doi.org/10.1088/1742-6596/251/1/012025.

[27] C. Hu, J. Zhang, Y. Bao, J. Wang, M. Li, Y.C. Zhou, In-situ reaction synthesis and decomposition of ta2alc, Int. J. Mat. Res. 99 (2008) 1, https://doi.org/10.3139/146.101598.
[28] I.M. Low, W.K. Pang, S.J. Kennedy, R.I. Smith, Study of high-temperature thermal stability of MAX phases in vacuum, Ceram. Eng. Sci. Proc. 31 (2010) 171–180, https://doi.org/10.1002/9780470944103.ch17.
[29] H. Zhang, Y. Zhou, Y. Bao, M. Li, Titanium silicon carbide pest induced by nitridation, J. Am. Ceram. Soc. 91 (2008) 494–499, https://doi.org/10.1111/j.1551-2916.2007.02018.x.
[30] M. Griseria, B. Tunca, T. Lapauw, S. Huang, L. Popescu, M.W. Barsoum, K. Lambrinou, J. Vleugels, Synthesis, properties and thermal decomposition of the ta4alc3 max phase, J. Eur. Ceram. Soc. 39 (2019) 2973–2981, https://doi.org/10.1016/j.jeurceramsoc.2019.04.021.
[31] M.W. Barsoum, H.-I. Yoo, I.K. Polushina, V. Yu, Rud, T. El-Raghy, Electrical conductivity, thermopower, and hall effect of ti3alc2, Ti4alN 3, and Ti3sic2, Phys. Rev. B 62 (2000) 10194–10199, https://doi.org/10.1103/PhysRevB.62.10194.
[32] P. Finkel, J.D. Hettinger, S.E. Lofland, M.W. Barsoum, T. El-Raghy, Magnetotransport properties of the ternary carbide ti3sic2:Hall effect, magnetoresistance, and magnetic susceptibility, Phys. Rev. B 65 (2001) 035113, https://doi.org/10.1103/PhysRevB.65.035113.
[33] M.W. Barsoum, T. El-Raghy, A progress report on ti3sic2, Ti3GeC2, and the H-phases, M2bx, J. Mater. Process. Technol. 5 (1997) 197.
[34] J.M. Ziman, Electrons and phonons, Clarendon Press, Oxford, 1960.
[35] P.B. Allen, in: J.R. Cehlikowsky and, S.G. Louie (Eds.), Quantum theory of real materials, 17, Kluwer, Boston, 1996, p. 219.
[36] A. Nassour, V. Mauchamp, W. Yu, T. Cabioch, L. Piraux, V. Gauthier-Brunet, S. Dubois, key role of electron-phonon interactions in the electronic conductivity of ti3sic2: experiment and ab initio calculations, Phys. Rev. B 93 (2016) 085119, https://doi.org/10.1103/PhysRevB.93.085119.
[37] G. Hug, P. Eklund, A. Orchowski, Orientation dependence of electron energy loss spectra and dielectric functions of ti3sic2 and ti3alc2, Ultramicroscopy 110 (2010) 1054–1058, https://doi.org/10.1016/j.ultramic.2010.05.007.
[38] C. Dhakal, S. Aryal, R. Sakidja, W.Y. Ching, Approximate lattice thermal conductivity of MAX phases at high temperature, J. Eur. Ceram. Soc. 35 (2015) 3203–3212, https://doi.org/10.1016/j.jeurceramsoc.2015.04.013.
[39] M.W. Barsoum, T. El-Raghy, C.J. Rawn, W.D. Porter, H. Wang, E.A. Payzant, C. R. Hubbard, Thermal properties of ti3sic2, J. Phys. Chem. Solids 60 (1999) 429–439, https://doi.org/10.1016/S0022-3697(98)00313-8.
[40] X. Qian, Y. Li, X. He, Y. Chen, S. Yun, Electrical and thermal properties of Ti3AlC2 at high temperature, J. Ceram. Sci. Technol. 2 (2011) 155–158, https://doi.org/10.4416/JCST2011-00018.
[41] M.W. Barsoum, I. Salama, T. El-Raghy, J. Golczewski, W.D. Porter, H. Wang, H. J. Seifert, F. Aldinger, Thermal and electrical properties of Nb2AlC, (Ti,Nb)2AlC and Ti2AlC, Metall. Mater. Trans. A 33 (2002) 2775–2782, https://doi.org/10.1007/s11661-002-0262-7.
[42] G.Ya Khadzhai, R.V. Vovk, T.A. Prichna, E.S. Gevorkyan, M.V. Kislitsa, A. L. Solovjov, Electrical and thermal conductivity of the ti3alc2 max phase at low temperatures, Low. Temp. Phys. 44 (2018) 451–456, https://doi.org/10.1063/1.5034158.
[43] M. Kohler, Zur magnetischen widerstandsänderung reiner metalle, Ann. Phys. 424 (1938) 211, https://doi.org/10.1002/andp.19384240124.
[44] J.M. Ziman, Electrons and Phonons: the Theory of Transport Phenomena in Solids, Cambridge University Press, Cambridge, UK, 2001.